

Wael Bachtá

Associate Professor
ISIR Université Pierre et
Marie Curie – CNRS,
Paris 75005, France
e-mail: wael.bachta@upmc.fr

Pierre Renaud¹

Associate Professor
e-mail: pierre.renaud@insa-strasbourg.fr

Edouard Laroche

Professor
e-mail: laroche@unistra.fr

Jacques Gangloff

Professor
e-mail: jacques.gangloff@unistra.fr

LSIIT Université de
Strasbourg – CNRS – INSA,
Strasbourg 67000, France

The Cardiolock Project: Design of an Active Stabilizer for Cardiac Surgery

Coronary artery bypass grafting is a common surgical procedure that requires a high level of accuracy. To perform this procedure on a beating heart, surgeons reduce the heart motion with passive stabilizers. These devices, however, lack accuracy. Indeed, marked residual motion of the area of interest can be observed. In this paper, we address the problem with the design of an active stabilizer, i.e., an active mechanism controlled to cancel any residual motion during the surgery. The design methodology is based on dynamic modeling of the stabilization task and an iterative design approach. In fact, Cardiolock 1, a prototype allowing partial compensation, has first been developed in order to refine the design requirements. Its design and evaluation are presented, before introducing Cardiolock 2, a device with full stabilization capabilities. It includes a remote center of motion and takes advantage of the vicinity of kinematic singularities to provide mechanical amplification. Numerical and experimental analyses of the device are introduced, illustrating the practical potential of the proposed design.

[DOI: 10.1115/1.4004117]

1 Introduction

1.1 Surgical Context. Coronary artery bypass grafting (CABG) is one of the most common surgical interventions in the field of heart surgery. It involves the suturing of grafts on coronary arteries of 1–2 mm of diameter, with more than ten knots around each graft. Therefore, high accuracy on the order of 0.1 mm is needed during knot tying. The most promising approach from a medical standpoint is to now perform CABG as a minimally invasive surgery (MIS) [1], with the insertion of instruments through small incisions, as well as without stopping the heart, as to suppress any harmful effect related to the use of heart–lung machines [2–4]. A passive mechanical device, known as a stabilizer, must be used in such conditions. For MIS, the Medtronic Octopus TE is the only commercially available stabilizer (Fig. 1). The device is mounted on the operating table and goes through a trocar located below the xiphoid process at the base of the sternum, up to the heart surface. Heart tissues are locally constrained by fingers located at the stabilizer tip using suction. The insufficient performance of such a device has been outlined in the medical field [1,5,6], with heart residual displacements of more than 4 mm [7].

1.2 Active Stabilization. The performance of a passive stabilizer is limited first by its geometry. The main shaft must be about 250 mm long, with a diameter on the order of 10 mm to be compatible with the MIS. The shaft must be hollow to integrate suction tubes and tissue irrigation tubes. Using simple strength-of-materials considerations, one can easily understand the limited performances of such a device, with a shaft deflection that exceeds the required accuracy. Second, any flexibility in the mounting of the stabilizer will increase the amplitude of the residual displacements. The necessary accuracy cannot be reached even with a dedicated experimental passive device [7].

We have therefore proposed the concept of active stabilization [8] in the Cardiolock project; high speed vision is used to observe the stabilizer tip, evaluate the presence of any residual displacement, and cancel it in real time using an active mechanism. In

other words, the displacement u_c (Fig. 2) needed to cancel the displacement of the stabilizer tip is obtained by the displacement u_a of an actuator. Any source of residual displacement can be compensated since the stabilizer tip, linked to the heart surface, is directly observed with the camera.

1.3 Related Work and Contributions. The principle of active compensation for beating heart surgery is original to our knowledge. It is indeed an alternate approach to active synchronization, where a robotized tool holder is controlled to follow the beating heart surface [9,10]. Since our approach relies on the idea of canceling in real time the effect of perturbations exerted on a smart device, some other related works can be found. In the medical field, the MiCRoN surgical assist device [11] aims to compensate for the surgeon's hand tremors, which are measured by accelerometers. A compliant actuation stage [12] is designed that includes piezoelectric actuators and holds a surgical instrument. The field of active compensation, including smart structures, contains other examples of active devices [13–15].

In this paper, we show that the surgical requirements can only be fulfilled with a custom mechanism. An active smart mechanism

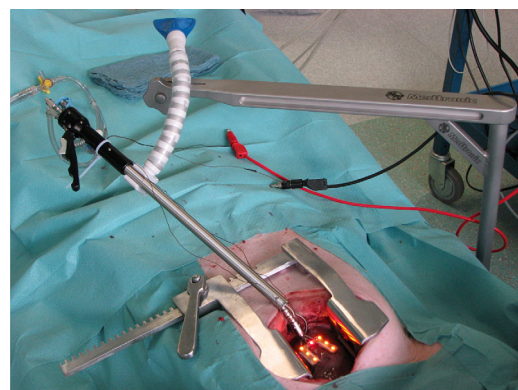


Fig. 1 The Medtronic Octopus TE. On the figure, the stabilizer tip is equipped with LEDs for an experimental evaluation on pigs of the residual displacements [7].

¹Corresponding author.

Contributed by the Mechanisms and Robotics Committee of ASME for publication in the JOURNAL OF MECHANICAL DESIGN. Manuscript received July 5, 2010; final manuscript received April 13, 2011; published online July 1, 2011. Assoc. Editor: Hong S. Yan.

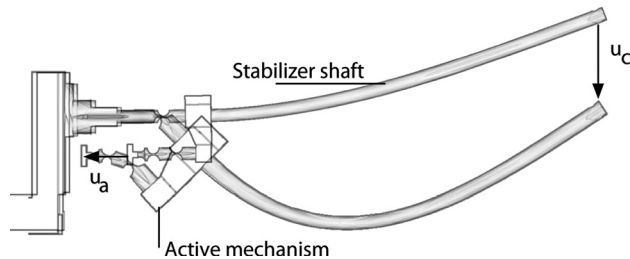


Fig. 2 Illustration of the principle of active compensation in the case of a bending of the stabilizer shaft

is therefore proposed, which includes a remote center of motion (RCM), allowing for the real time compensation of stabilizer shaft motion with sufficient dynamics. A design methodology is introduced. It is based on dynamic modeling of the stabilization task and on an iterative design: a first prototype, Cardiolock 1, providing partial compensation, has been designed to help to refine the requirements. The final device, Cardiolock 2, is based on an original piezoactuated mechanism relying on the use of a parallel structure near singularity as a mechanical amplifier. Numerical and experimental assessments of the two prototypes are conducted to show that Cardiolock 2, the proposed active stabilizer, fulfills the application requirements.

The paper is organized as follows. The main design requirements are introduced in Sec. 2. The design methodology is given in Sec. 3, with the development of the analytical modeling. Then, the design of Cardiolock 1, a proof-of-concept device to refine the design requirements, is presented in Sec. 4. The design of Cardiolock 2, the device with full stabilization capability, is finally developed in Sec. 5 before concluding.

2 Design Requirements

2.1 Stabilizer Kinematics. The surgical access location cannot be modified. As a consequence, the general set-up of the passive stabilizer is preserved. The base of the active stabilizer is mounted rigidly on the operation table by means of a passive positioning system (Fig. 3), for an insertion through a trocar located below the xiphoid process. The trocar limits the diameter of the stabilizer shaft to 10 mm, and the shaft length is chosen equal to 250 mm, such as on the Octopus TE, to allow for the access to any area of the heart.

The success of the suture relies on the accuracy of the insertion of the needle. Thus, the stabilizer aims to suppress the translations of the beating heart surface. Variations of the surface orientation, however, are limited and do not affect the procedure's accuracy. Previous in vivo experimental analysis [7] has shown that the forces exerted by the heart on the stabilizer create large moments on the base of the stabilizer that introduce stabilizer tip displacement, in addition to those due to the bending of the shaft. The sig-

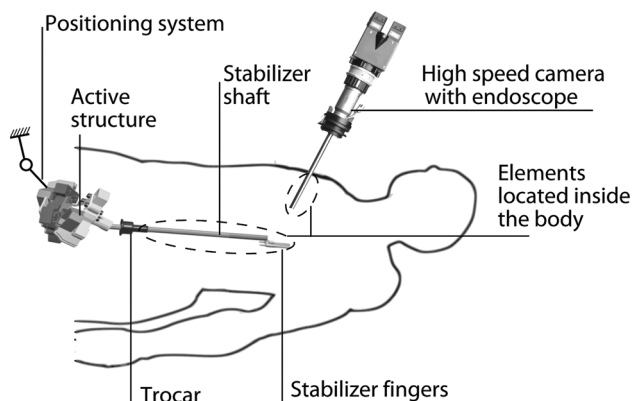


Fig. 3 Schematic representation of the active stabilizer set-up

nificant heart displacements are thus in the two directions perpendicular to the shaft axis. The active stabilizer must, as a consequence, exhibit two degrees of freedom (DOF) in translation at the stabilizer tip. The displacements needed to do the compensation are of small amplitude and can therefore be obtained by achieving two rotations with a RCM around the trocar center. This is of particular interest; in such a situation, the forces exerted by the trocar on the stabilizer will not create any moment around the rotational axes. The control of the device will, hence, be significantly simplified, since we only need to focus on the influence of the beating heart surface.

Mobilities of the stabilizer fingers with respect to the body are needed to properly orientate the fingers on the myocardium surface. The design of the passive subsystem to provide this motion is not considered in the scope of this paper. However, the influence of its possible flexibility is analyzed.

2.2 Stabilizer Dynamics. The velocity of a free beating heart surface has been experimentally studied on pigs [16,17] and humans [18]. The velocities remain quite similar: a free heart motion is characterized by velocities up to 0.12 m s^{-1} . Accelerations in the case of pig hearts [16,17] can reach 6 m s^{-2} , and we can consider, due to the anatomical similarities, that such accelerations can also be observed in a human heart. In our context, the heart is constrained by a stabilizer. Velocities and accelerations will of course be significantly reduced. Their exact values depend on the mechanical structure and the control of the device. In the following, we voluntarily use the values obtained for a free heart motion as upper bounds for the design.

Experiments on pigs with heart size comparable to that of human hearts have been performed to investigate the nature of the interaction between a beating heart surface and a stabilizer [19]. The force in the plane perpendicular to the stabilizer shaft is equal to 4 N. Because of the anatomical similarities [17,18,20,21], it can be expected that the interaction forces for a human will be close to the forces measured on a pig. Therefore, we assume that the stabilizer can be used for the compensation of forces up to 4 N in any direction perpendicular to the stabilizer shaft.

2.3 Surgical Requirements. The asepsis of the device must be ensured. The most efficient [22] and widespread sterilization technique is the use of an autoclave. We, therefore, consider that all the active elements of the stabilizer have to remain outside the body of the patient, wrapped in a sterile bag while the stabilizer shaft and fingers can be sterilized using an autoclave.

3 Design Methodology

3.1 The Design Problem. The stabilizer kinematics, the required dynamics, and the forces exerted by the heart on the stabilizer are defined. The actuation of the stabilizer and its synthesis are now developed. The aim of the active stabilizer is to suppress any small displacement measured by vision in real time. To avoid any backlash in the system, the device is based on a compliant mechanism. For the same reason, piezoelectric stack actuators are selected. Among the possible actuators [23], piezoelectric stacks are the only ones that do not introduce any backlash or any friction in the system, and they have the high dynamics needed for real time compensation. The stabilizer tip position is controlled through the rotation of the shaft, by means of an actuator located outside the body. The high resolution of the piezoelectric stacks will furthermore allow for fine control of the position of the stabilizer tip.

Piezoelectric stack actuators provide a linear motion, known to be of small amplitude. The stabilizer design, therefore, consists in selecting adequate actuators and designing a transformation mechanism to convert their linear motion into a rotation of the stabilizer shaft. In the first step, a dynamic model of the stabilization task is introduced to determine admissible actuators. The

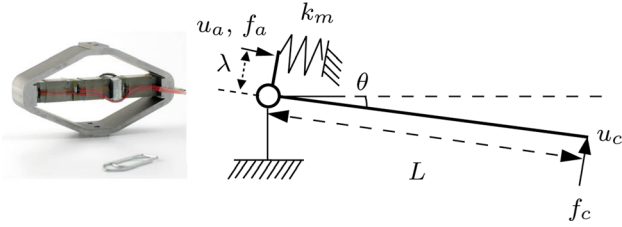


Fig. 4 Actuator for the compensation (left) and modeling of the task (right)

synthesis of the compliant mechanism is achieved in the second step, using an iterative design with the development of Cardiolock 1.

3.2 Initial Determination of the Actuators

3.2.1 Modeling. The stabilization task is considered along 1 DOF. A transformation mechanism is needed to obtain the rotation θ of the stabilizer shaft from the piezoelectric actuator displacement u_a (Fig. 4). Small displacements are considered, so that the two variables θ and u_a are linearly related by

$$\theta = \frac{u_a}{\lambda} \quad (1)$$

with λ a characteristic length of the mechanism. The transformation mechanism is a compliant mechanism of stiffness k_m , whose inertia is neglected. The stabilizer shaft movement is then described by

$$I\ddot{\theta} = \lambda(f_a - k_m u_a) - f_c L \quad (2)$$

where I is the inertia of the shaft, f_c is the force applied by the cardiac muscle, and L is the shaft length. The force f_a applied by the actuator and its displacement u_a are linked by the actuator stiffness k_a [24]

$$f_a = f_0 - k_a u_a \quad (3)$$

with f_0 the blocked force, i.e., the force obtained for a null displacement, which is dependent on the voltage applied to the piezoelectric stack. Combining Eqs. (1)–(3), the displacement $u_c = L\theta$ at the stabilizer tip can be given by

$$\frac{I}{\lambda L} \ddot{u}_c = f_0 - (k_a + k_m) \frac{\lambda}{L} u_c - \frac{f_c L}{\lambda} \quad (4)$$

The displacement u_c needed to achieve the compensation is initially considered equal to the amplitude of the stabilizer shaft deflection under the cardiac force f_c

$$u_c = \frac{f_c L^3}{3EI_q} \quad (5)$$

with I_q being the area moment of inertia of the shaft and E its Young modulus. Finally, Eq. (4) can be rewritten to describe the compensation of the stabilizer deflection

$$\left((k_a + k_m) f_c \frac{L^2}{3EI_q} \right) \lambda^2 - f_0 \lambda + \left(\frac{I}{L} u_c + f_c L \right) = 0 \quad (6)$$

3.2.2 Actuator Selection. Equation (6) is a quadratic equation in λ , the characteristic length transforming the actuator displacement in the stabilizer shaft rotation. For a given actuator, k_a and f_0 are known. The actuator selection is adequate if, for a given cardiac force f_c and a given heart acceleration u_c , there exists at least one positive value of λ . If the discriminant of Eq. (6) is positive, a

range of values of λ exists that allows for the compensation. The minimum value is constrained by the actuator force needed to obtain equilibrium of the shaft, and the maximum value is constrained by the displacement needed to compensate the deflection.

Increasing the parameter k_m leads to the decrease of the discriminant of Eq. (6). To determine admissible actuators, we first consider $k_m = 0$ to check that a solution can be obtained at least in that case. The parameters (I, L, E, I_q) are known: the shaft is made of stainless steel and its geometry is constrained by the application. The force f_c is known from Sec. 2.2. Actuators manufactured by Cedrat Technologies [24] are considered (e.g., see APA120ML in Fig. 4). These actuators are composed of a piezoelectric stack integrated in a mechanical amplifier. Using Eq. (6), a dozen actuators can then fit the need, and for the most compact admissible actuator (APA60S, dimensions 15 mm \times 29 mm \times 5 mm), the length λ can be comprised between 17 mm and 45 mm.

3.2.3 Influence of Additional Flexibilities. Let μ be the value of the compliance describing additional flexibilities that can exist in the system in addition to the shaft flexibility. It may come from the passive positioning system on which is mounted the stabilizer, or the fingers that constrain the myocardium surface. The displacement to be compensated due to the cardiac force, u_c , is then equal to

$$u_c = \frac{f_c L^3}{3EI_q} + \mu f_c = \left(\frac{L^3}{3EI_q} + \mu \right) f_c \quad (7)$$

Equation (6) then becomes

$$\left((k_a + k_m) \left(\frac{L^2}{3EI_q} + \frac{\mu}{L} \right) f_c \right) \lambda^2 - f_0 \lambda + \left(\frac{I}{L} u_c + f_c L \right) = 0 \quad (8)$$

The introduction of additional flexibilities decreases the discriminant of Eq. (8) and logically lowers the range of admissible values of λ for a given actuator. Once the amplitude of additional flexibilities is defined, it is therefore possible to determine the range of acceptable actuators.

3.3 Device Synthesis. The design now involves choosing the characteristic length λ and implementing an adequate transformation mechanism. If λ is increased, the rotation of the shaft is decreased. For a given force f_c and stiffness k_m , the force developed during the compensation by the actuator will hence decrease. A high value of λ is likely to lead to a less compact design, if for instance a simple lever mechanism is chosen. On the contrary, if a low value of λ is considered, the actuator will act more as a force generator than a displacement generator. The compensation can be performed; however, the increase of the actuator force can create higher stresses in the transformation mechanism. The value of the stresses in the mechanism therefore has to be taken into account in order to perform the synthesis of the stabilizer: it is not possible to optimize the choice of the actuator and the value of the characteristic length independently from the mechanism synthesis.

The dynamic properties of the device will have a strong influence on the stabilization efficiency. The structure eigenfrequencies will limit the control bandwidth and, consequently, the device dynamics. Moreover, as outlined in Sec. 3.2.3, the value of the additional flexibilities to take into account need to be evaluated to design a device with sufficient stabilization performances. An iterative design methodology is, therefore, proposed to achieve the device synthesis: in Sec. 4, a proof-of-concept prototype, Cardiolock 1, is designed and evaluated in order to define precisely the requirements in terms of flexibilities to be compensated and eigenfrequencies.

4 Cardiolock 1—Lessons From a 1 DOF Device

Cardiolock 1 is considered for experiments on pigs only, with compensation along a single DOF. Experiments with a MIS approach are not possible because of the animal anatomy. As a

consequence, we do not take into account the need for a rotation around the trocar expressed in Sec. 2.1.

4.1 Initial Determination of Actuators. To deal with initial uncertainties about the experimental conditions, the value of the cardiac force is increased by 50%, i.e., 6 N, and an additional flexibility equal to 50% of the shaft flexibility is taken into account. From Eq. (8), only six actuators from Cedrat Technologies can be chosen. The APA120ML is selected for its small size. The admissible range of values of λ is then equal to [2; 45] mm if a null value of k_m is considered.

4.2 Selection of a Transformation Mechanism. The actuator translation is converted into a rotation by means of a slider-crank mechanism (Fig. 5). The actuator is the slider that is linked to the base of the mechanism to avoid the influence of the inertia of its body. The connecting rod is chosen parallel to the stabilizer shaft in its nominal position, so that the force applied by the heart induces only a force perpendicular to the actuator. The objective is to use the actuator as an actuated prismatic joint, without an additional compliant joint, to limit the introduction of additional stiffnesses that will increase k_m and consequently reduce the set of admissible lengths λ . In the nominal position defined by $\theta = \beta = 0$, the characteristic length is equal to the parameter e .

4.3 Mechanism Synthesis. The mechanism is represented in Fig. 5, using a pseudo rigid body model (PRBM, [25]). The connecting rod that has a length d_2 , the crank on which the stabilizer shaft is mounted, is defined by the parameters e and d_1 . On the figure, the displacements are amplified for sake of clarity, but the stabilizer exhibits only small displacements with respect to the nominal configuration. The revolute joints of the mechanism are modeled as revolute joints with torsion springs, to model the elasticity of the compliant joints. The joints are considered identical, with a symmetric right-circular profile [26] of minimum thickness t and stiffness k_r . The flexibility of the shaft is modeled by a spring of stiffness k_s that is related to the shaft properties.

The stiffness k_m can be related to the stiffness k_r , using a simple static analysis

$$k_m = 2 \frac{k_r}{e^2} \left(1 - \frac{d_1}{d_2} + \frac{d_1^2}{d_2^2} \right) \quad (9)$$

Equations (4) and (7) constitute two constraints to be fulfilled. The stresses in the joints must also remain lower than a threshold defined by the material. Maximum stress in each joint is expressed by [27]

$$\sigma_i = \frac{M_i t}{2J_i} \quad (10)$$

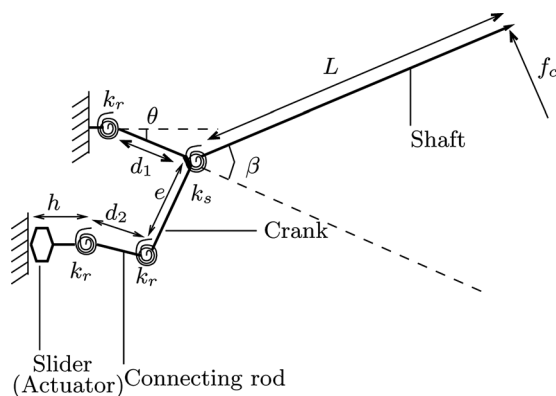


Fig. 5 Slider-crank mechanism for the Cardilock 1 transformation mechanism

with σ_i the stress in the joint i , $i \in [1, 3]$. M_i designates the moment applied on the joint. The parameters t and J_i , respectively, represent the minimum thickness of the compliant joint and the second moment of area at the smallest section of the joint. The maximum stress value is chosen equal to 100 MPa, a threshold chosen according to the endurance limit of the considered stainless steel, of type 316L, and the fact that the stress will vary at the cardiac frequency between a null value and the maximum stress introduced in Eq. (10)

$$\sigma_i \leq 100 \text{ MPa}, i \in [1, 3] \quad (11)$$

Equations (4), (7), and (11) must be fulfilled simultaneously. Parameters (t, e, d_1, d_2) are obtained by using a nonlinear constraint optimization in order to simultaneously ensure all these conditions. The optimization criterion is the size of the device, defined by the product between e and $\text{Min}(d_1, d_2 + h)$ with h the size of the actuator (Fig. 5). During the optimization, parameters are constrained in intervals: $t \geq 0.5$ mm to allow the machining of the compliant joints, $e \geq 30$ mm, $d_1 \geq 10$ mm and $d_2 \geq 18$ mm for manufacturability and assembly. The constrained nonlinear optimization is based on the use of a SQP method integrated in the MATLAB Optimization Toolbox (Mathworks, Natick, MA). Finally, the best geometry is defined by $[t, e, d_1, d_2] = [0.5, 30, 10, 18]$ mm. With these values, the characteristic length λ is equal to 30 mm. The maximum stress is equal to 80 MPa, which is below the maximum admissible stress. The CAD view of the corresponding system is introduced in Fig. 6.

4.4 Finite Element Analysis. The validity of the analytical model is first verified by comparing the computed value of k_m to the value obtained using finite element analysis (FEA) with Pro/Mechanica. The mesh contains 2000 tetrahedral P-elements [28], with a maximum order of 6. The stiffness values are consistent, with a relative difference of 5%. The distal displacement u_c predicted with the analytical model is equal to 1.48 mm when the actuator is performing its maximal excursion in the absence of cardiac force. This is also in accordance with the value obtained from FEA, equal to 1.47 mm.

The ability of the device to achieve the compensation task is studied in a second step. The dynamics of the compensation task can indeed be handled easily in a static FEA simulation by coupling the simulation with the analytical model. From Eq. (4), it can be seen that if some distal acceleration \ddot{u}_c is required, the maximum excursion of the stabilizer tip is reduced by $\ddot{u}_c / (\lambda^2 (k_a + k_m))$. This value is rather small, in the order of 8 μm , and one can see in Fig. 7 that when the maximum excursion of the actuator is used in the presence of the maximum cardiac force, the stabilizer is able to compensate for its own deflection and also for an additional displacement equal to 0.75 mm. This value is satisfactory, since it is beyond 50% of additional flexibility considered initially.

The first four eigenfrequencies, evaluated using FEA, are equal to 46.6 Hz, 66.3 Hz, 294.2 Hz, and 370.7 Hz. The first two frequencies correspond to the first eigenmode of the shaft with, respectively, a lateral and vertical contribution of the transformation mechanism. The third and fourth modes are due to the second eigenmode of the stabilizer shaft with a contribution of the transformation mechanism.

The maximum Von Mises stress is equal to 125 MPa when the compensation is performed. The value is significantly higher than



Fig. 6 CAD view of the the Cardilock 1 prototype

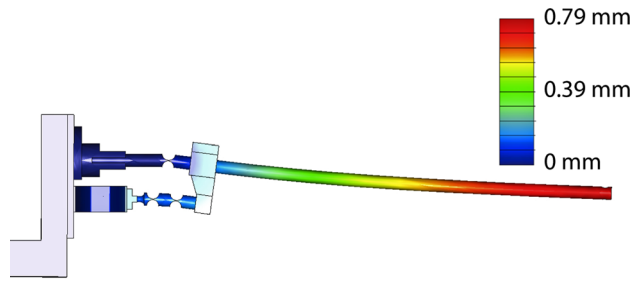


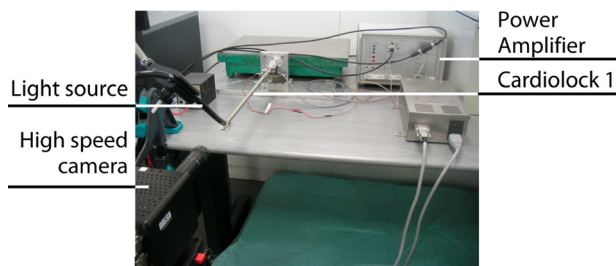
Fig. 7 FEA of Cardiolock 1: The maximum displacement of the actuator is applied simultaneously to a 6 N force on the stabilizer shaft. Displacements, indicated in mm, are amplified for sake of clarity.

the value defined in Sec. 4.3. The difference comes from the simplified expression used in Eq. (10). The value remains admissible for the material during first experiments.

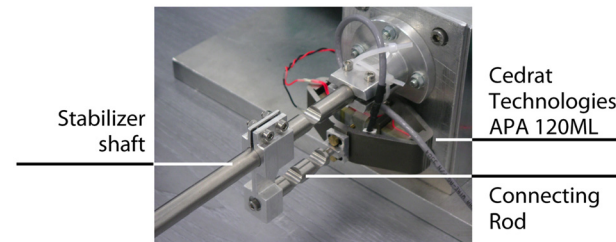
4.5 Experimental Analysis. The Cardiolock 1 prototype is represented in Fig. 8. The compliant elements are obtained using the CNC machining.

The stabilizer tip displacement is evaluated with a Dalsa CAD-6 (256 × 256 pixels, 300 fps) camera equipped with a Navitar Precise Eye lens (Fig. 8). The measurement accuracy is then in the order of 7 μm. The lens is chosen for the compensation task, with a field-of-view that indeed does not allow the measurement of the maximum tip excursion. However, for a control voltage between -1 V and 5.5 V, which represents 75% of the actuator range, the stabilizer tip exhibits a displacement with very good linearity (Fig. 9), and by extrapolation, the displacement amplitude is experimentally determined to be equal to 1.39 mm, which is comparable to the value of 1.47 mm estimated using FEA.

The stiffness of the device can be easily evaluated by applying a force on the stabilizer tip and measuring its displacement. Experiments show that significant differences appear with respect to FEA results: the prototype has a stiffness of 6.5 N/mm, whereas the value obtained numerically is equal to 8.5 N/mm. Additional tests have shown that even though the base of the device is of large dimensions, it introduces an additional flexibility in the system that can explain the experimental/FEA difference.



(a) The experimental set-up



(b) Close-up view on the compliant mechanism

Fig. 8 Cardiolock 1 prototype during the experimental evaluation

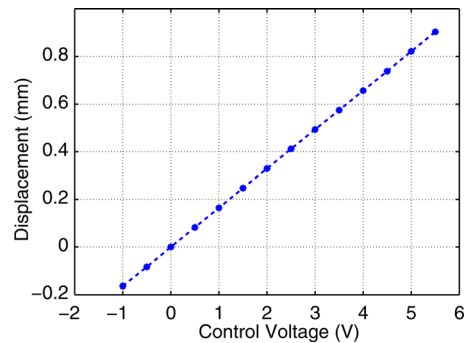


Fig. 9 Cardiolock 1 tip displacement as a function of the control voltage

The first two eigenfrequencies are equal to 40 Hz and 59 Hz. The first eigenfrequency corresponds to the lateral movement, and the second to the vertical movement of the stabilizer tip. Eigenmodes are similar to those estimated from FEA, but at rather different eigenfrequencies. A posteriori numerical simulations show that these differences can be explained by the sensitivity of the mechanism to the quality of the assembly of the connecting rod of the transformation mechanism. Indeed, modifying by 0.2 mm the diameter of the mounting surface of the connecting rod on the actuator decreases in FEA, the eigenfrequencies from 46.6 Hz to 45 Hz and from 66.3 Hz to 59 Hz. The second eigenfrequency is then equal to the experimental value. The first eigenfrequency is probably also sensitive to the flexibility of the base of the device that has been observed experimentally during the stiffness evaluation.

In vivo experiments on pigs have demonstrated the efficiency of the device [8]. The device was mounted on a medical robot, instead of being directly mounted on the operation table. This robot is indeed not designed to be a mechanical holder and it presents significant flexibilities. These experimentations have allowed us to determine the control bandwidth that is needed to perform the stabilization. This bandwidth is related to the frequency content of the cardiac force, and one can observe that having the first eigenfrequency beyond 40 Hz is satisfactory. The residual displacements to be compensated can also be evaluated with the experimental set-up. Displacements of 0.25 mm in addition to the stabilizer deflection have been observed, due to the significant flexibility of the medical robot. This value can thus be considered as an upper bound for the displacements due to additional flexibilities.

With the Cardiolock 1 prototype, the flexibilities to take into account in the design of the stabilizer have been evaluated, as well as the required minimum value of the first eigenfrequency of the device. It is also interesting to note the high sensitivity of the device to the number of parts in the device, which lowers the stiffness and the eigenfrequencies.

5 Cardiolock 2—Design of the Final Active Stabilizer

5.1 The RCM Architecture. Cardiolock 2, the final device, is designed to fulfill all the requirements expressed in Sec. 2.1. In particular, the mechanism must exhibit rotations with respect to a RCM at the location of the trocar. Several mechanisms with a RCM and serial or parallel architectures have been proposed in prior literature. Parallel spherical structures can be obtained by using several legs, each having a spherical movement [29]. In other mechanisms, the sphericity is obtained by a judicious arrangement of the joints [30,31]. For the cited architectures, the center of motion could coincide with the trocar. In all these configurations, revolute and sometimes spherical joints have to be manufactured with a spatial arrangement to obtain a compliant architecture. Thus, the manufacturing complexity is very high. Moreover, when sphericity is due to special conditions on the joint positions, manufacturing errors and flexibilities can cause the loss of sphericity. In that case, it is difficult to establish which displacements are finally controlled.

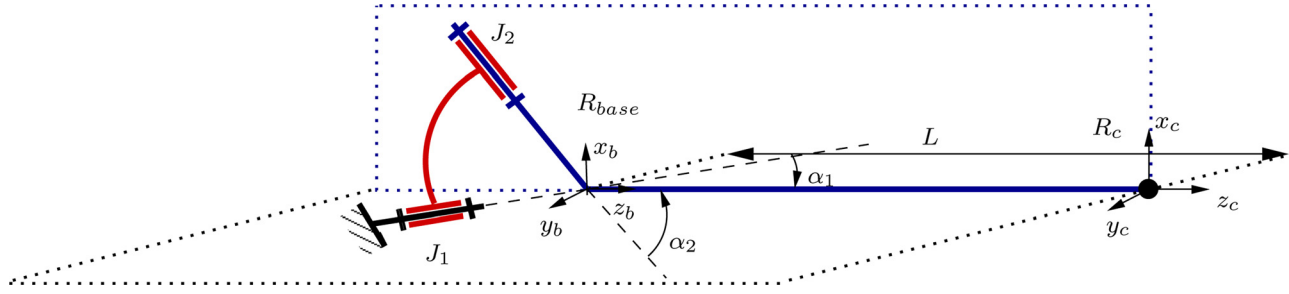


Fig. 10 Kinematic scheme of the serial architecture of Cardiolock 2

Additionally, experimental evaluation of Cardiolock 1 has shown that the device dynamic behavior is very sensitive to the linkage assembly. The choice has therefore been made to minimize the complexity of the architecture assembly and to promote simplicity by considering a 2 DOF serial spherical architecture. Indeed, since the rotations of the stabilizer beam are of small amplitude, it is interesting to consider the special arrangement represented in Fig. 10, which allows us to get a decoupled behavior in the represented nominal configuration. In Fig. 10, one can see that the first revolute joint J_1 axis lies with the shaft axis in a horizontal plane and provides an end-effector velocity in the x_c direction. The second joint J_2 axis lies with the shaft in a vertical plane, so that the y_c direction velocity is obtained. This decoupling will simplify the dynamic control of the system.

The Jacobian matrix that relates the joint velocities $(\dot{\theta}_1, \dot{\theta}_2)^T$ to the end-effector velocities (\dot{x}, \dot{y}) is only a function of the angles α_1 and α_2 , since the beam length L is constrained by the medical requirements

$$\begin{pmatrix} \dot{x} \\ \dot{y} \end{pmatrix} = \begin{pmatrix} L \sin(\alpha_1) & 0 \\ 0 & L \sin(\alpha_2) \end{pmatrix} \begin{pmatrix} \dot{\theta}_1 \\ \dot{\theta}_2 \end{pmatrix} \quad (12)$$

The Jacobian matrix also provides the relationship between small revolute joint rotations and end-effector displacements. For a given set of end-effector displacements, the actuated joints rotations decrease when angles α_1 and α_2 increase. From a dynamic point-of-view, parameters α_1 and α_2 should be minimized in order to obtain a more compact structure, with lower inertias. However, because the piezoelectric actuators used to control the revolute joints have a limited stroke, the values of α_1 and α_2 must also consider the actuation of each joint.

5.2 Initial Determination of Actuators. In the nominal position, the mechanism presents a kinematic decoupled behavior. The dynamic model introduced in Eq. (4) can therefore be used to describe the behavior of each joint. The displacement to be compensated is still described by Eq. (5). The displacement that can be performed with each piezoelectric actuator is however now a function of the angles α_1 and α_2 . For symmetry reasons, we will consider these angles to be the same, and denote them both equal to the parameter α . The end-effector displacement that can be reached in each direction is then equal to

$$u_c = \frac{u_a}{\lambda} L \sin(\alpha) \quad (13)$$

Equations (4) and (6) can then be rewritten as

$$\begin{cases} \frac{I}{\lambda L \sin(\alpha)} \ddot{u}_c = f_0 - (k_a + k_m) \frac{\lambda}{L \sin(\alpha)} u_c - \frac{f_c L \sin(\alpha)}{\lambda} \\ \left(\frac{k_a + k_m}{3EI_q \sin(\alpha)} \right) \lambda^2 - f_0 \lambda + \left(\frac{I}{L \sin(\alpha)} u_c + f_c L \sin(\alpha) \right) = 0 \end{cases} \quad (14)$$

For the joint J_2 , the inertia I still corresponds mainly to the inertia of the stabilizer shaft. For the joint J_1 , the inertia of the transformation mechanism of J_2 needs to be taken into account. The stiffness k_m may also influence the choice of λ . As a consequence, it is quite difficult to further use the dynamic model at this stage of the device design. However, it is interesting to note that the range of admissible values of λ for a given actuator is narrower for Cardiolock 2 than for Cardiolock 1 for equal performances. The actuator APA120ML can ensure sufficient performances for the joint J_2 only if $\lambda \in [0.5, 21]$ mm, for an angle α in the order of 25 deg. This range is obtained if the equivalent stiffness k_m of the transformation mechanism is null and will be even lower if k_m increases. For the joint J_1 , the range will also be reduced because of the larger inertia. Transformation mechanisms with a small characteristic length λ must be designed.

5.3 Transformation Mechanisms: Singularities for Amplification. For a simple mechanism such as the slider-crank mechanism chosen for Cardiolock 1, the characteristic length λ is linked to the length e (Fig. 5). If we want to increase the rotation for a given actuator translation, the parameter λ has to be lowered. The decrease of λ remains limited; the mechanism stiffness is strongly reduced for small values of λ if we consider out-of-plane forces. Actually, some closed-loop mechanisms, or more generally parallel architectures, can enable a stiffer structure to minimize any uncontrollable displacements, at the same time as allowing for large rotations from the displacement provided by the piezo actuator. The idea is to use kinematic singularities to get these properties. For a parallel mechanism, the actuator velocities $\dot{\mathbf{q}}$ and the end-effector velocity $\dot{\mathbf{X}}$ are linked by the relationship

$$\mathbf{J}_q \dot{\mathbf{q}} = \mathbf{J}_X \dot{\mathbf{X}} \quad (15)$$

where \mathbf{J}_X is rank deficient in a parallel singularity [32] That means $\dot{\mathbf{X}} \neq 0$ can be obtained with $\dot{\mathbf{q}} = 0$ and, in the vicinity of that singularity, one can tend to increase the ratio between actuators and end-effector velocities. We use this property for the design of the transformation mechanism. Kinematic singularities of parallel structures are usually avoided, and indeed seldom used [33–35] It is interesting to note that indeed, in the field of actuator design, the properties of parallel singularities are often used when designing linear displacement amplifiers [36–38] The proposed solutions are based on the use of parallel singularity, for instance such as in bridge-type mechanisms [38], but without explicit identification of the phenomenon or a robotic formulation. Since the equivalent of a revolute joint is needed, with equal stiffness in all the directions, one can immediately think of a planar parallel structure, whose thickness can be selected to obtain the desired out-of-plane stiffnesses. In Fig. 11, the 3PRR mechanism is represented in a configuration close to singularity. The rotation ε is the only parameter that avoids to be completely in singularity.

The points $A_i, i \in [1, 3]$ are controlled by actuated prismatic joints. Their directions are defined by unit vectors $\mathbf{u}_i, i \in [1, 3]$, and q_i denotes the prismatic joint position. The end-effector pose is defined by the position (x, y) of E and its orientation θ . For such

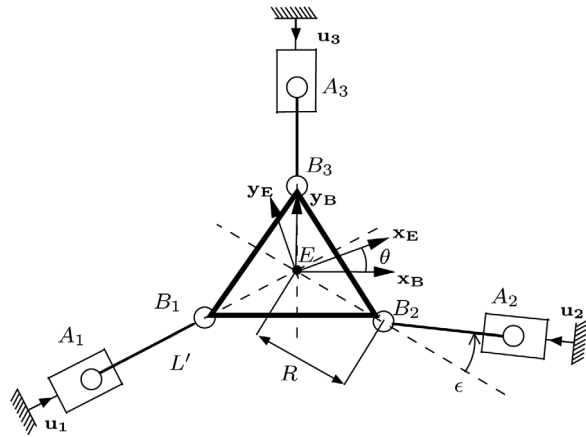


Fig. 11 Planar 3PRR close to parallel singularity

a mechanism, the expression of \mathbf{J}_X and \mathbf{J}_q (Eq. (15)) can be easily derived, using equiprojectivity properties

$$\mathbf{J}_X = \begin{pmatrix} A_1B_1|_x & A_1B_1|_y & (A_1B_1 \times B_1E)|_z \\ A_2B_2|_x & A_2B_2|_y & (A_2B_2 \times B_2E)|_z \\ A_3B_3|_x & A_3B_3|_y & (A_3B_3 \times B_3E)|_z \end{pmatrix} \quad (16)$$

$$\mathbf{J}_q = \begin{pmatrix} \mathbf{u}_1 \cdot A_1B_1 & 0 & 0 \\ 0 & \mathbf{u}_2 \cdot A_2B_2 & 0 \\ 0 & 0 & \mathbf{u}_3 \cdot A_3B_3 \end{pmatrix}$$

with \mathbf{z} being the unit vector perpendicular to the mechanism plane, and $(\dot{x}, \dot{y}, \dot{\theta})^T$ being the vector of operational velocities. In the configuration represented in Fig. 11, the first and third elements of the third column of \mathbf{J}_X become equal to zero: the elements A_1B_1 and A_3B_3 are aligned with, respectively, the vectors A_1E and A_3E . Thus, if we consider zero velocities for the mechanism legs 1 and 3, the end-effector velocity (\dot{x}, \dot{y}) is equal to zero, and the velocity of the actuator 2 is linked to the rotational speed $\dot{\theta}$

$$\dot{\theta} = \frac{1}{R \sin(\epsilon)} \dot{q}_2 \quad (17)$$

where $R = \|EB_2\|$ (Fig. 11). The parallel structure is equivalent to an actuated revolute joint of axis (E, \mathbf{z}) . The ratio between the velocity \dot{q}_2 and the velocity $\dot{\theta}$, or between the small displacement δq_2 and the small rotation $\delta \theta$, is inversely proportional to ϵ . The characteristic length λ is equal to $R \sin(\epsilon)$ and we can then easily tune its value by modifying ϵ to obtain a high rotation/translation ratio. Hence, we obtain a structure with interesting stiffness properties when considering forces in the plane of the mechanism, and a high transformation ratio between the actuator velocity and the rotational speed. This ratio is set by the value of the angle, ϵ , that represents the closeness to the singularity. Since we consider a compliant mechanism, out-of-plane stiffness is controlled by the width of the mechanism.

Finally, we can consider Cardiolock 2 as a serial spherical architecture, each actuated revolute joint being obtained by means of a planar parallel structure in a configuration parallel to parallel singularity. The parallel structures are controlled with piezoelectric actuators and designed as compliant mechanisms. For such mechanisms, the PRBM approach enables us to use the previously introduced kinematic analysis. The synthesis of the planar structure, however, must be achieved by taking into account the stresses in the joints.

5.4 Mechanism Synthesis

5.4.1 Objectives and Design Parameters. The amplitude of the cardiac force encountered during experiments with Cardiolock 1

remained in the order of 4 N. A safety factor is still introduced by considering maximum forces in the two directions of compensation equal to 6 N and the maximum accelerations introduced in Sec. 2.2. Based on the experiments with Cardiolock 1, the deflection due to the additional flexibilities is equal to 0.25 mm.

Identical transformation mechanisms are considered to simplify the design and manufacturing of the system. The geometry of a transformation mechanism (Fig. 11) is defined by three variables: (R, ϵ, L') . Including the angle α between the revolute joint axis and the stabilizer shaft (Fig. 10), four geometric parameters need therefore to be selected. In addition to these parameters, the width of the planar transformation mechanisms and the profile of the compliant joints included in these mechanisms have to be defined.

5.4.2 Main Guidelines

Choice of materials: During the compensation, the amplitude of the rotation of the joints J_1 and J_2 is obtained from the value of the stabilizer deflection. The displacement of each compliant transformation mechanism is therefore imposed, and the induced stresses must remain below the endurance limit of the material. The Young's modulus E governs the stress intensity and the endurance limit σ_d defines the maximum admissible stress. As a consequence, the ratio E/σ_d is considered to select the most adequate material for the transformation mechanisms. Aluminum alloy 7075T6, which combines an interesting E/σ_d ratio and good machining properties, is chosen for the mechanism. A stainless steel hollow shaft is chosen, to allow for the integration of suction and tissue irrigation tubes. The selected tube has an external diameter of 10 mm and an inner diameter of 7 mm.

Influence of the design parameters: Because of the mechanism geometry, developing analytical models of the stresses in the mechanism seems very complex and of limited efficiency. The design has thus been based on an iterative approach, using FEA to evaluate the behavior of the device. The choice of design variables is simplified by first analyzing the influence of the following design parameters:

- The width w of the transformation mechanisms is chosen to ensure a sufficient out-of-plane stiffness. The width is limited by the inertia and the equivalent stiffness k_m (Eq. (14)).
- To remain compatible with a CNC machining of the system, the minimum thickness of the compliant joints is chosen to equal 0.5 mm. The compliant revolute joints that compose of the transformation mechanisms are described in Fig. 12.
- The rotation of the transformation mechanism end-effector is a function of the radius R and the angle ϵ (Eq. (17)). The choice of these two parameters is linked to the choice of the angle α , since they define the relationship between the piezoelectric actuator displacement and the stabilizer shaft tip

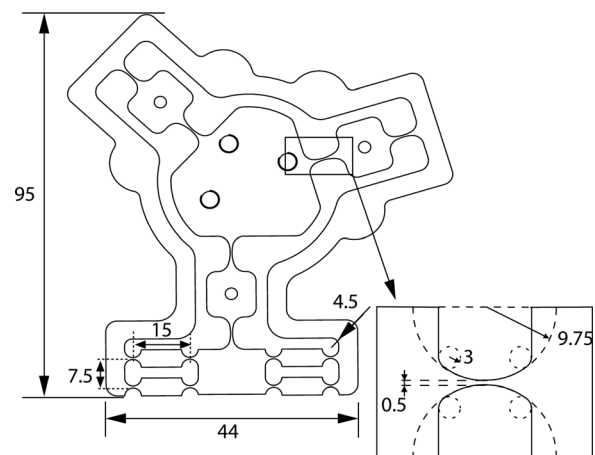


Fig. 12 Dimensions in millimeters of the transformation mechanism and the compliant prismatic joint

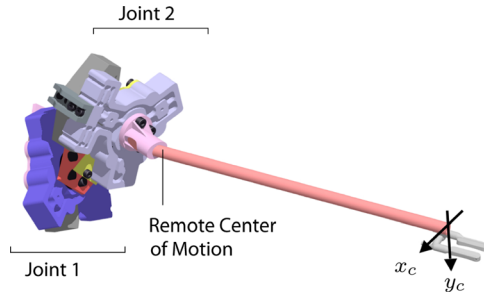


Fig. 13 CAD view of the Cardiolock 2 device

displacement. The rotation θ' of the elements $A_i B_i$, $i \in [1, 3]$ is also, with a first-order approximation, a function of the radius R and the length L'

$$\theta' = \frac{R}{L'} \theta$$

The stresses in the compliant joints are functions of the rotation θ' . This rotation should be minimized to lower the stresses. Its minimization is, however, limited: the radius R must be large enough to allow the assembly of the device, and the increase of the length L' induces the increase of the transformation mechanism's inertia.

- The stiffness of the amplification structure integrated in the actuator is not sufficient to ensure a linear displacement of the point B_2 (Fig. 11). A compliant prismatic joint needs to be added. The compliant joint is based on 4-bar linkages in a symmetrical arrangement (Fig. 12). To limit the increase of the stiffness k_m , the joints have the minimum thickness. The length of the 4-bar linkages is chosen to respect the maximum allowable stress in the joints (Fig. 12).

Final design: The stabilizer is represented in Figs. 13 and 14. Values of the geometrical parameters are reported in Table 1. With the selected geometry, the characteristic length is equal to only 4.5 mm. This value is much lower than in the case of Cardiolock 1, due to the value of the Jacobian matrix expressed in Eq. (12). The actuators are APA120ML, similar to the one used for Cardiolock 1.

5.5 Finite Element Analysis. FEA is performed with Pro/Mechanica. The mesh contains 19500 tetrahedral P-elements [28], with a maximum order of 7. The workspace of the stabilizer tip is equal to 1.67 mm \times 1.28 mm. The workspace is not fully symmetric because of a higher flexibility of the element to which the actuator of J_2 is connected. Using a static numerical analysis and the analytical model expressed in Eq. (14), it is possible to assess the compensation task in dynamic conditions, similar to the procedure in Sec. 4. Due to the required accelerations, the reachable displacements of the stabilizer tip are reduced by 0.06 mm and 0.01 mm along the x_c and y_c directions, respectively (Fig. 10). The stabilizer, however, is still able to compensate a 6 N force in two directions, as well as additional deflections equal to 0.45 mm and 0.15 mm along the x_c and y_c directions. These values are very close to those measured during experiments with Cardiolock 1,

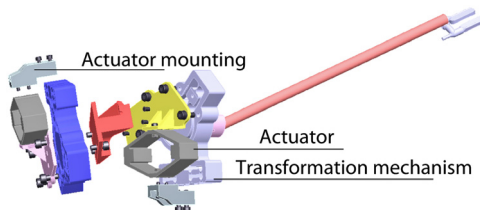


Fig. 14 Exploded view of Cardiolock 2

Table 1 Geometrical parameters of Cardiolock 2

Parameter	α	R	L'	ε	w
Value	25 deg	20 mm	14 mm	13 deg	20 mm

which validate the performances of the stabilizer. The first two eigenfrequencies of the device are equal to 52 Hz and 74 Hz. The first eigenmode corresponds mainly to a rotation around the axis of J_1 . The second eigenmode is due to the resonance of the stabilizer shaft with a simultaneous bending of the transformation mechanism of J_1 . Using the results obtained with Cardiolock 1, these values appear compatible with the control bandwidth needed for the compensation.

During compensation, the maximum Von Mises stress is in the order of 190 MPa. This value is encountered in the compliant revolute joints of the transformation mechanisms, and is mostly a uniaxial stress during the flexure of the joints. Such a stress is acceptable for the 7075T6 aluminum alloy in fatigue, with a fatigue lifetime that can be estimated to be $>10^7$ cycles.

5.6 Experimental Results. The Cardiolock 2 prototype is manufactured using CNC machining (Fig. 15). Because of material availability, the stabilizer shaft currently has an inner diameter equal to 8 mm. The stabilizer flexibility is increased, and comparisons with FEA are achieved considering the modified geometry.

The vision system used for Cardiolock 1 is used to evaluate the workspace of Cardiolock 2. The stabilizer tip position in the camera frame is represented in Fig. 16 for input voltages between 0 and 3 V that represent 35% of the displacement range. The displacements in the image validate the desired kinematic decoupled behavior: each joint can produce a translation in the image, without being influenced by the other joint. A slight perpendicularity error of 4 deg. appears between the displacements due to each joint. It is, however, difficult to position finely the camera with respect to the stabilizer tip, and the perpendicularity error may either come from manufacturing errors or a misalignment of the camera with the stabilizer.

The experimentation shows that the mounting of the base of the stabilizer slightly lowers the performance of the first joint with respect to the FEA results. The workspace of the prototype is indeed equal to 1.28 mm \times 1.28 mm, which means the displacement in the y_c direction corresponds to the value issued from FEA and displacement in the x_c direction is 23% lower. The compensation can be performed in static conditions for a force equal to 5.5 N in the x_c direction and 6 N in the y_c direction. The compensation capability in the y_c direction corresponds to the value obtained from FEA, but it is 18% lower in the x_c direction.

The eigenmodes are observed by exciting the system with the piezoelectric actuators. The first two eigenfrequencies are equal to 48 Hz and 52 Hz. These values are close to those obtained with a simulation taking into account the experimental mounting of the prototype: the first two eigenfrequencies are then equal to 48 Hz and 56 Hz. The second eigenmode is hardly observable during the



Fig. 15 Global view of the Cardiolock 2 device

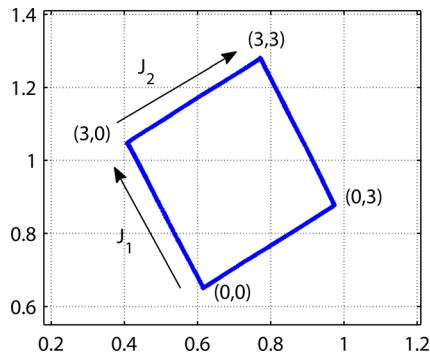


Fig. 16 Displacements of the Cardiolock 2 shaft tip in the camera frame for input voltages equal to 3 V (position in millimeters, voltage values indicated into brackets for the two joints)

experimentation if the actuator of J_1 is used, which is in accordance with the FEA results: the second eigenmode is due to the resonance of the stabilizer shaft and the bending of the compliant transformation mechanism that is not influenced by the movement of the actuator of J_1 . The experimental directions of displacement of the stabilizer tip are also in accordance with the FEA results.

As a summary, the experimental results show that the current prototype of Cardiolock 2 has sufficient performance for the compensation in two directions during *in vivo* experiments on pigs; the device can compensate for the deflections due to 4 N forces, with the required accelerations. Experiments demonstrate that in this case additional deflections up to 0.35 mm and 0.43 mm, respectively, in the x_c and y_c directions can also be compensated. If a stabilizer shaft with an inner diameter of 7 mm is used, as initially considered, the device will allow for the compensation of deflections due to cardiac forces up to 6 N in two directions, including additional flexibility of the same amplitude as those observed during the initial *in vivo* experiments with Cardiolock 1.

6 Conclusion

In this paper, the mechanical design of an active stabilizer for beating heart minimally invasive CABG has been presented. In a first step, the dynamic modeling of the compensation task has been introduced to predetermine the actuators. In a second step, the iterative design approach of the stabilizer has been presented. Cardiolock 1, the first prototype allowing for partial compensation, has been used to refine the dynamic requirements and the necessary compensation performances. Afterward, Cardiolock 2, the device with full stabilization capability, has been introduced. It fulfills the dynamic requirements as well as the need for a mechanism exhibiting a remote center of motion. In order to obtain sufficient performances, the proposed architecture is based on a serial mechanism with original amplification mechanisms designed by using the kinematic properties of parallel mechanisms. Numerical and experimental results demonstrate the efficiency of the device. The control of Cardiolock 2 will now be investigated before intensive *in vivo* experimentation. Another perspective concerns the improvement of the accuracy and the robustness of the vision-based evaluation of the beating heart displacements. Recent work on the observation of natural landmarks on the heart [39] is promising.

References

- [1] Loisanec, D., Nakashima, K., and Kirsch, M., 2005, "Computer-Assisted Coronary Surgery: Lessons From an Initial Experience," *Interact. Cardiovasc. Thorac. Surg.*, **4**(5), pp. 398–401.
- [2] Mack, M., 2000, "Pro: Beating-Heart Surgery for Coronary Revascularization: Is it the Most Important Development Since the Introduction of the Heart–Lung Machine?," *Ann. Thorac. Surg.*, **70**(5), pp. 1779–1781.
- [3] Patel, N., Deodhar, A., Grayson, A., Pullan, D., Keenan, D., Hasan, R., and Fabri, B., 2002, "Neurological Outcomes in Coronary Surgery: Independent Effect of Avoiding Cardiopulmonary Bypass," *Ann. Thorac. Surg.*, **74**(2), pp. 400–406.

- [4] Boyd, W. D., Desai, N. D., Rizzo, D. F. D., Novick, R. J., McKenzie, F. N., and Menkis, A. H., 1999, "Off-Pump Surgery Decreases Post-Operative Complications and Resource Utilization in the Elderly," *Ann. Thorac. Surg.*, **68**(4), pp. 1490–1493.
- [5] Dogan, S., Aybek, T., Risteski, P., Mierdl, S., Stein, H., Herzog, C., Khan, M., Dzemali, O., and Moritz, A., 2004, "Totally Endoscopic Coronary Artery Bypass Graft—Initial Experience With an Additional Instrument Arm and an Advanced Camera System," *Surg. Endosc.*, **18**(11), pp. 1587–1591.
- [6] Kappert, U., Cichon, R., Schneider, J., Gulielmos, V., Ahmadsade, T., Nicolai, J., Tugtekin, S.-M., and Schueler, S., 2001, "Technique of Closed Chest Coronary Artery Surgery on the Beating Heart," *Eur. J. Cardio-thorac. Surg.*, **20**(4), pp. 756–769.
- [7] Bachta, W., Renaud, P., Laroche, E., Forgione, A., and Gangloff, J., 2008, "Cardiolock: An Active Cardiac Stabilizer, First *In Vivo* Experiments Using a New Robotized Device," *Comput. Aided Surg.*, **13**(5), pp. 243–254.
- [8] Bachta, W., Renaud, P., Laroche, E., Forgione, A., and Gangloff, J., 2007, "Design and Control of a New Active Cardiac Stabilizer," *IEEE/RSJ International Conference on Intelligent Robots and Systems*, San Diego, USA, pp. 404–409.
- [9] Nakamura, Y., Kishi, K., and Kawakami, H., 2001, "Heartbeat Synchronization for Robotic Cardiac Surgery," *IEEE International Conference on Robotics and Automation*, Seoul, Korea, Vol. 2, pp. 2014–2019.
- [10] Ginhoux, R., Gangloff, J., de Mathelin, M., Soler, L., Sanchez, M., and Marescaux, J., 2005, "Active Filtering of Physiological Motion in Robotized Surgery Using Predictive Control," *IEEE Trans. Rob.*, **21**(1), pp. 67–79.
- [11] Riviere, C., Ang, W. T., and Khosla, P., 2003, "Toward Active Tremor Canceling in Handheld Microsurgical Instruments," *IEEE Trans. Rob. Autom.*, **19**(5), pp. 793–800.
- [12] Choi, D., and Riviere, C., 2005, "Flexure-Based Manipulator for Active Handheld Microsurgical Instrument," *27th Annual International Conference of the IEEE Engineering in Medicine and Biology Society*, Shanghai, China, pp. 2325–2328.
- [13] Frecker, M. I., 2003, "Recent Advances in Optimization of Smart Structures and Actuators," *J. Intell. Mater. Syst. Struct.*, **14**(5), pp. 207–215.
- [14] Janocha, H., 2007, *Adaptronics and Smart Structures: Basics, Materials, Design, Applications*. Springer, Berlin, Heidelberg.
- [15] Trease, B., and Kota, S., 2009, "Design of Adaptive and Controllable Compliant Systems With Embedded Actuators and Sensors," *ASME J. Mech. Des.*, **131**(11), p.111001.
- [16] Ortmaier, T., Groger, M., Boehm, D., Falk, V., and Hirzinger, G., 2005, "Motion Estimation in Beating Heart Surgery," *IEEE Trans. Biomed. Eng.*, **51**(10), pp. 1729–1740.
- [17] Cuvillon, L., Gangloff, J., de Mathelin, M., and Forgione, A., 2005, "Toward Robotized Beating Heart tecaB: Assessment of the Heart Dynamics Using High-Speed Vision," *International Conference on Medical Image Computing and Computer-Assisted Intervention*, Palm Springs, USA, Vol. 8, pp. 551–558.
- [18] Shechter, G., Resar, J., and McVeigh, E., 2006, "Displacement and Velocity of the Coronary Arteries: Cardiac and Respiratory Motion," *IEEE Trans. Med. Imaging*, **25**(3), pp. 369–375.
- [19] Bachta, W., Renaud, P., Laroche, E., Gangloff, J., and Forgione, A., 2007, "Cardiolock: An Active Cardiac Stabilizer—First *In Vivo* Experiments Using a New Robotized Device," *International Conference on Medical Image Computing and Computer Aided Intervention*, Brisbane, Australia, LNCS-4791, pp. 78–85.
- [20] Miller, A., Bohr, D., Schork, A., and Terris, J., 1979, "Hemodynamic Responses to Doca in Young Pigs," *Hypertension*, **1**(6), pp. 591–597.
- [21] Kovacic, V., Rogulvic, L., Bacic, B., and Bosnjak, T., 2003, "Mean Arterial Pressure and Pulse Pressure are Associated With Different Clinical Parameters in Chronic Haemodialysis Patients," *J. Hum. Hypertens.*, **17**(5), pp. 353–360.
- [22] Yoon, J. H., Yoon, B. C., Cho, S. C., Lee, H. L., Lee, O. Y., Choi, H. S., and Hahm, J. S., 2009, "Comparison of Sterilization Methods Using Autoclave and Ethylene Oxide Gas in Reprocessing of Reusable Endoscopy Biopsy Forceps," *Gastrointest. Endosc.*, **69**(5), p. AB219.
- [23] Ouyang, P., Clement, R., Zhang, W., and Yang, G., 2007, "Micro Motion Devices Technology: The State of Arts Review," *J. Adv. Manuf. Technol.*, **38**(5), pp. 463–478.
- [24] CedratTechnologies, 2008, *Cedrat Piezo Product Catalogue*.
- [25] Howell, L., 2001, *Compliant Mechanisms*. Wiley, New York.
- [26] Lobontiu, N., 2003, *Compliant Mechanisms—Design of Flexure Hinges*, CRC Press, Florida.
- [27] Pham, H., and Chen, I., 2002, "Kinematics, Workspace and Static Analyses of 2-dof Flexure Parallel Mechanism," *International Conference on Control, Automation, Robotics and Vision*, Singapore, pp. 968–973.
- [28] Gagnon, Y., 2008, *ProMechanica Structure Wildfire 4.0 Elements and Applications—Part I*, Schriff Development Corporation, Mission, KS.
- [29] Gosselin, C., and Angeles, J., 1989, "The Optimum Kinematic Design of a Spherical Three-Degree-of-Freedom Parallel Manipulator," *J. Mech., Transm. Autom. Des.*, **111**(2), pp. 202–207.
- [30] Fang, Y., and Tsai, L., 2004, "Structure Synthesis of a Class of 3-dof Rotational Parallel Manipulators," *IEEE Trans. Rob. Autom.*, **20**(1), pp. 117–121.
- [31] Gregorio, R. D., 2004, "Kinematics of the 3-RSR Wrist," *IEEE Trans. Rob. Autom.*, **20**(4), pp. 750–754.
- [32] Gosselin, C., and Angeles, J., 1990, "Singularity Analysis of Closed-Loop Kinematic Chains," *IEEE Trans. Rob. Autom.*, **6**, pp. 281–290.
- [33] Ronchi, S., Company, O., Pierrot, F., and Fournier, A., 2005, "High Resolution Flexible 3-RRR Planar Parallel Micro-Stage in Near Singular

- Configuration for Resolution Improvement,” IEEE International Conference on Industrial Technology, Hong Kong, pp. 395–400.
- [34] Ranganath, R., Nair, P. S., Mruthyunjaya, T. S., and Ghosal, A., 2006, “A Force-Torque Sensor Based on a Stewart Platform in a Near-Singular Configuration,” *Mech. Mach. Theory*, **39**(9), pp. 971–998.
- [35] Stoughton, R., and T. A., 1992, “Kinematic Optimization of a Chopsticks-Type Micromanipulator,” Japan-USA Symposium on Flexible Automation, USA, pp. 4472–4477.
- [36] Niezrecki, C., Brei, D., Balakrishnan, S., and Moskalik, A., 2001, “Piezoelectric Actuation: State of the Art,” *Shock Vib. Digest*, **33**(4), pp. 269–280.
- [37] Ouyang, P., Zhang, W., and Gupta, M., 2005, “Design of a New Compliant Mechanical Amplifier,” ASME International Design Engineering Technical Conference, Long Beach, USA, Vol. 7A, pp. 15–24.
- [38] Yao, H.-W., Ma, S.-M., Wang, L.-Q., and Zhong, Z., 2006, “Analysis of the Displacement Amplification Ratio of Bridge-Type Flexure Hinge,” *Sens. Actuators*, **132**(2), pp. 730–736.
- [39] Richa, R., Bo, A., and Poignet, P., 2010, “Robust 3d Visual Tracking for Robotic-Assisted Cardiac Interventions,” International Conference on Medical Image Computing and Computer-Assisted Intervention, Beijing, China, pp. 267–274.